Semiconductor Science and Technology

PAPER

Bandgap tuning of GaAs/GaAsSb core-shell nanowires grown by molecular beam epitaxy

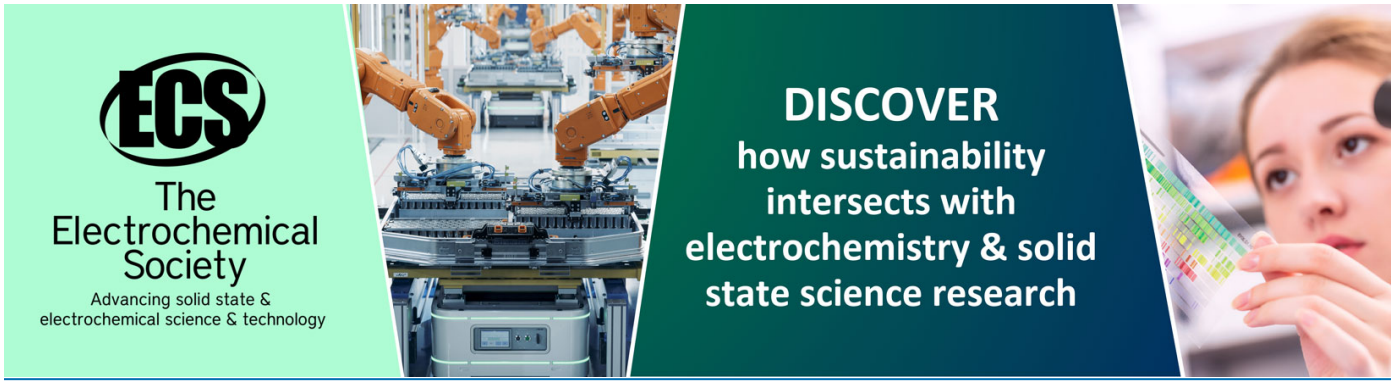

IOP Publishing Semiconductor Science and Technology
Semicond. Sci. Technol. **30** (2015) 105036 (10pp) doi:10.1088/0268-1242/30/10/105036

Bandgap tuning of GaAs/GaAsSb core-shell nanowires grown by molecular beam epitaxy

Pavan Kumar Kasanaboina[1], Sai Krishna Ojha[1], Shifat Us Sami[2], C Lewis Reynolds Jr[3], Yang Liu[3] and Shanthi Iyer[1,2]

[1] Department of Electrical and Computer Engineering, North Carolina A&T State University, Greensboro, NC 27411, USA
[2] Nanoengineering, Joint School of Nanoscience and Nanoengineering, NCA&T State University, Greensboro, NC 27401, USA
[3] Department of Materials Science and Engineering, North Carolina State University, Raleigh, NC 27695, USA

E-mail: iyer@ncat.edu (Shanthi Iyer)

Received 8 July 2015, revised 17 August 2015
Accepted for publication 19 August 2015
Published 21 September 2015

Abstract

Semiconductor nanowires have been identified as a viable technology for next-generation infrared (IR) photodetectors with improved detectivity and detection across a range of energies as well as for novel single-photon detection in quantum networking. The GaAsSb materials system is especially promising in the 1.3–1.55 μm spectral range. In this work we present band-gap tuning up to 1.3 μm in GaAs/GaAsSb core–shell nanowires, by varying the Sb content using Ga-assisted molecular beam epitaxy. An increase in Sb content leads to strain accumulation in shell manifesting in rough surface morphology, multifaceted growths, curved nanowires, and deterioration in the microstructural and optical quality of the nanowires. The presence of multiple PL peaks for Sb compositions $\geqslant$12 at.% and degradation in the nanowire quality as attested by broadening of Raman and x-ray diffraction peaks reveal compositional instability in the nanowires. Transmission electron microscope (TEM) images show the presence of stacking faults and twins. Based on photoluminescence (PL) peak energies and their excitation power dependence behavior, an energy-band diagram for GaAs/GaAsSb core–shell nanowires is proposed. Optical transitions are dominated by type II transitions at lower Sb compositions and a combination of type I and type II transitions for compositions $\geqslant$12 at.%. Type I optical transitions as low as 0.93 eV (1.3 μm) from the GaAsSb for Sb composition of 26 at.% have been observed. The PL spectrum of a single nanowire is replicated in the ensemble nanowires, demonstrating good compositional homogeneity of the latter. A double-shell configuration for passivation of deleterious surface states leads to significant enhancement in the PL intensity resulting in the observation of room temperature emission, which provides significant potential for further improvement with important implications for nanostructured optoelectronic devices operating in the near-infrared regime.

Keywords: nanowires, bandgap tuning, core-shell, molecular beam epitaxy

(Some figures may appear in colour only in the online journal)

1. Introduction

The flexibility offered by the one-dimensional structure of nanowires in band-gap engineering, material design architecture, and the wide choice of substrates have made it an attractive candidate for a variety of device applications. Nanowire (NW) arrays are ideally suited to meet the demands of the third-generation of infrared (IR) photodetectors for imaging with high prospects for improving detectivity, providing better spatial resolution, and offer the potential for multispectral detection by integration of different NW arrays on the same substrate and the possibility of hybrid integration

of driver electronics and detectors on the same chip. In particular, wavelengths in the near-infrared region (NIR), 1.3–1.55 μm, have also been of great interest for telecommunications, and there has been continued demand for improvement in these photodetectors. In recent years, devices with high spatial resolution and single-photon detection have become even more important due to the increasing research interest in quantum networking.

Two ternary material systems that have been extensively investigated in thin-film devices operating at these wavelengths are GaAsSb [1–3] and InGaAs [4, 5]. The GaAsSb (III-V-V) system offers distinct advantages over InGaAs (III-III-V) due to (a) suppressed Auger recombination, (b) longer electron lifetime, and (c) less dependency of the electronic structure on its alloy configuration due to the presence of a single group III element [6]. In nanowires, the advantage of a single group III element is more apparent due to the commonly used vapor-liquid-solid (VLS) growth mechanism for NW growth. Large differences in the In and Ga diffusion rates can lead to considerable compositional inhomogeneity in InGaAs nanowires. Furthermore, the GaAsSb system has the advantage that the surfactant nature of Sb can be exploited to improve the structural and optoelectronic properties.

Several reports have been published on both axial and radial heterostructured growth of gold-assisted and gold-free growth of GaAs/GaAsSb nanowires [7–11]. The focus of the majority of the work has been on crystal structure and insertion of GaAsSb layers in GaAs. Recently, Todorovic *et al* [12] investigated the optical properties of GaAsSb inserts in GaAs nanowires for different lengths of the ternary insert, and band-gap tuning to 1.2 eV was demonstrated by varying Sb composition using Au-assisted molecular beam epitaxy (MBE). Our group reported a similar study with longer inserts and using Ga-assisted MBE [13]. We also recently reported [14] the effect of growth temperature of the shell on the properties of core–shell GaAs/GaAsSb nanowires. Au-free self-catalyzed Ga assisted growth offers the advantage of not only eliminating the Au-induced defects but also suppressing undesirable axial growth during shell growth. It should be noted that a GaAsSb material system belongs to a highly mismatched alloy (HMA) system and the other HMA systems that have been the subject of investigations in the NW configurations are GaP/GaPN [15] and GaAs/GaAsN [16] core–shell nanowires, though the band-gaps have slightly higher energy values of 1–2 eV.

The focus of this investigation is a comprehensive understanding of the effects of Sb variation in the Ga-assisted MBE growth of GaAs/GaAsSb in the core–shell configured nanowires for next-generation photodetectors in the telecommunication wavelength range. The impact of Sb variation on morphology, strain, composition, band gap, and band alignment have been studied in detail using a variety of characterization techniques. These are the first reports to our knowledge of achieving PL emission wavelength of 1.3 μm in Ga-assisted GaAsSb core–shell nanowires with prospects of further improvement in PL efficiency demonstrated by passivating the GaAsSb surface via a double-shell configuration.

2. Experimental details

All nanowires were grown on P-type Si (111) substrates using an EPI 930 solid source MBE system with valved As and Sb cracker sources. The growth of GaAs/GaAsSb core–shell nanowires was comprised of two steps. First, core GaAs nanowires were grown using the VLS mechanism with Ga as the catalyst at 620 °C. Ga-assisted NW growth was initiated by impinging Ga flux on the substrate for 15 s prior to the opening of the As_4 flux with a beam- equivalent pressure of 4.8×10^{-6} Torr. After growing the core NW for a given duration, the Ga droplets on the tips of the nanowires were solidified to avoid further axial growth during shell growth. GaAsSb shell growth was then initiated after lowering the growth temperature. The shell growth temperature was varied between 550 °C–590 °C and the Sb flux was varied from 2.4×10^{-7} to 2.8×10^{-6} Torr. For the growth of double-shell GaAs/GaAsSb/GaAs nanowires, the Sb flux was terminated prior to the commencement of the second GaAs shell growth.

Scanning electron microscope (SEM) imaging was carried out using a Carl Zeiss Auriga-BU FIB field emission scanning electron microscope (FESEM) with an energy-dispersive x-ray spectrometer for compositional analysis. X-ray diffraction scans (XRD) were performed using Bruker's D8 Discover instrument with a DaVinci diffractometer in the standard Bragg–Brentano para-focusing configuration. X-rays from the Cu Kα source were not filtered and thus contained both $K_{\alpha 1}$ and $K_{\alpha 2}$ components. The scanning transmission electron microscopy (STEM) analysis was performed on a probe aberration-corrected FEI Titan G2 system operated at 200 kV. The bright-field TEM, selected-area electron diffraction (SAED), and high-resolution TEM (HRTEM) were characterized on a JEOL 2010F microscope operated at 200 kV. Micro-photoluminescence (μ-PL) measurements were conducted in a low vibration closed cycle optical cryostat from Montana Cryostation with the sample chamber extended away from the cryostat. The sample chamber was interfaced with a fiber-coupled confocal microscope from Horiba Jobin Yvon, Inc., with a 633 nm He-Ne laser as the excitation source. The PL signal from the sample was then dispersed using a 0.32 m double-grating monochromator with liquid nitrogen cooled InGaAs detector for detection using conventional lock-in techniques. Raman spectroscopy was carried out at room temperature in a Horiba Jobin Yvon LabRam ARAMIS Raman microscope using a He-Ne laser with 633 nm excitation wavelength. The Raman signal was detected using a multichannel air-cooled charge-coupled device.

3. Results and discussion

Figure 1(a) shows an SEM image of highly vertical core GaAs nanowires on Si (111) substrate with a density in the range of 6–8 μm^{-2}. The nanowires are 4 μm long with diameters ranging from 70–80 nm. Figure 1(b) depicts typical

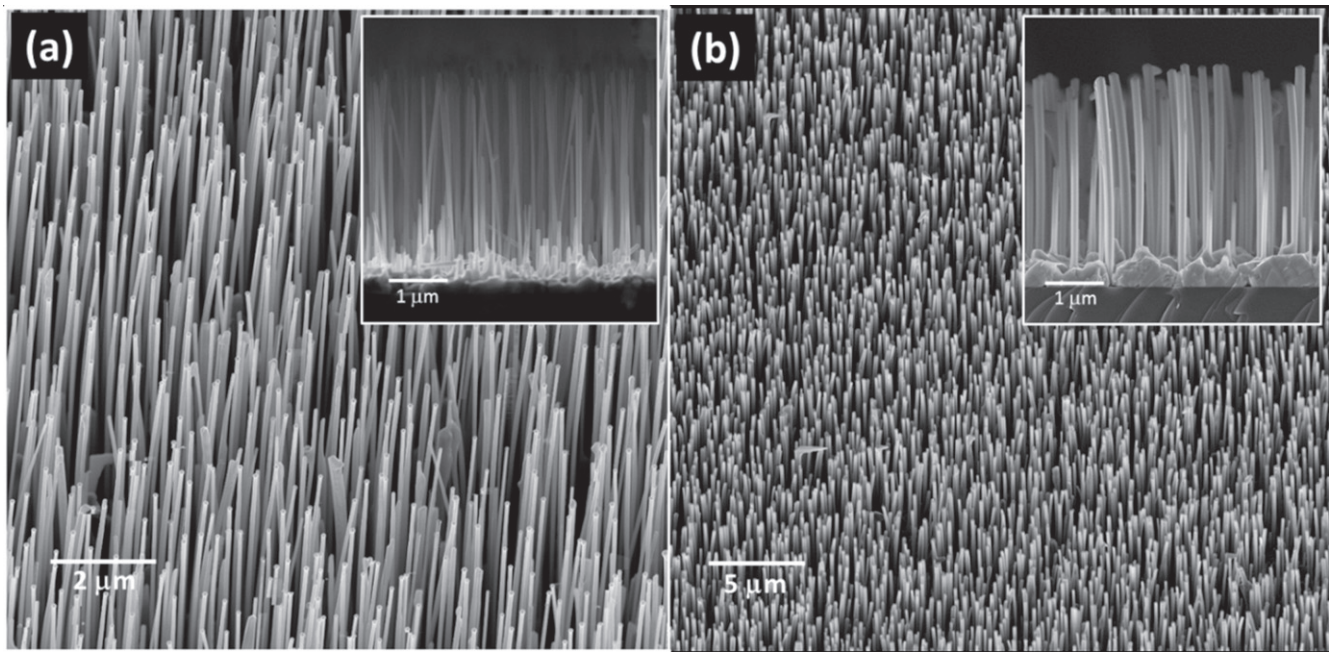

Figure 1. (a) Core GaAs nanowires and (b) core–shell GaAs/GaAsSb nanowires. The insets show the respective side views.

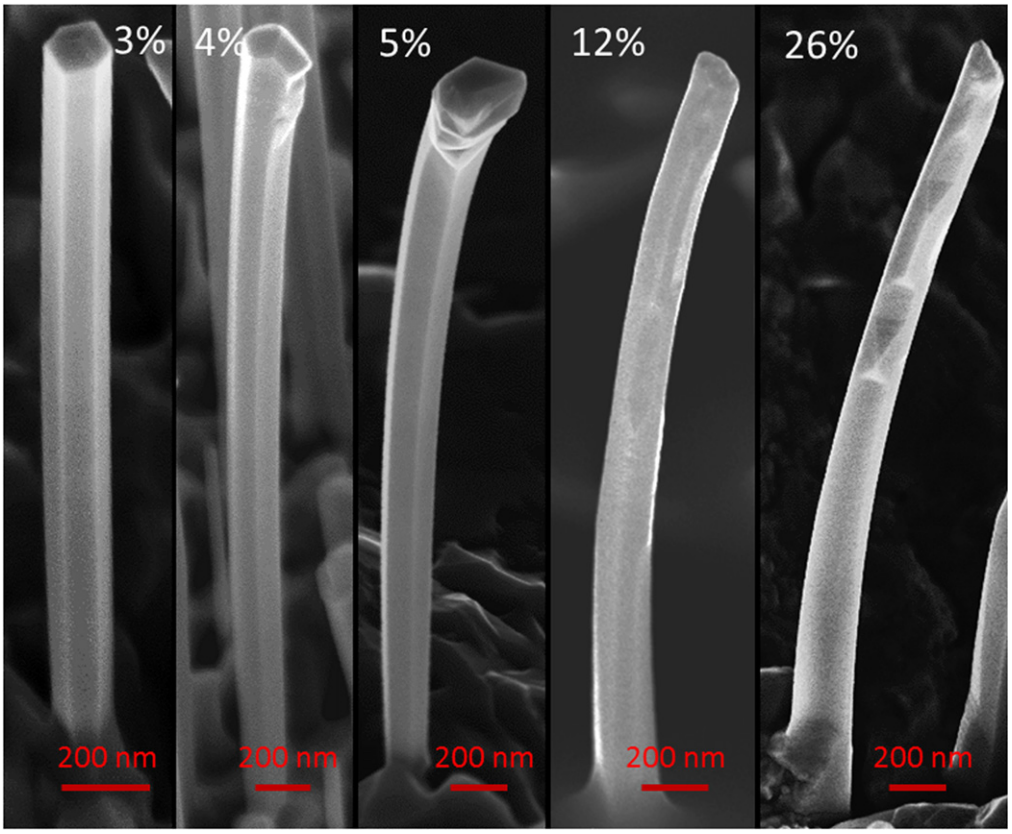

Figure 2. SEM micrographs of single GaAs/GaAsSb core–shell nanowires for different Sb compositions.

GaAs/GaAsSb core–shell nanowires with length and diameters of 4 μm and 180 nm, respectively.

Figure 2 displays the SEM images of the GaAs/GaAsSb core–shell nanowires with increasing Sb incorporation up to 26 at.%. The smooth morphology and well-defined hexagonal faceted top view cross-section observed in nanowires with low Sb content of 3 at.% is transformed to a rougher morphology with different overgrown side facets and elongated hexagonal cross-section with increasing Sb content, as shown in figure 2. The diameter of the NW increases from 183 nm to

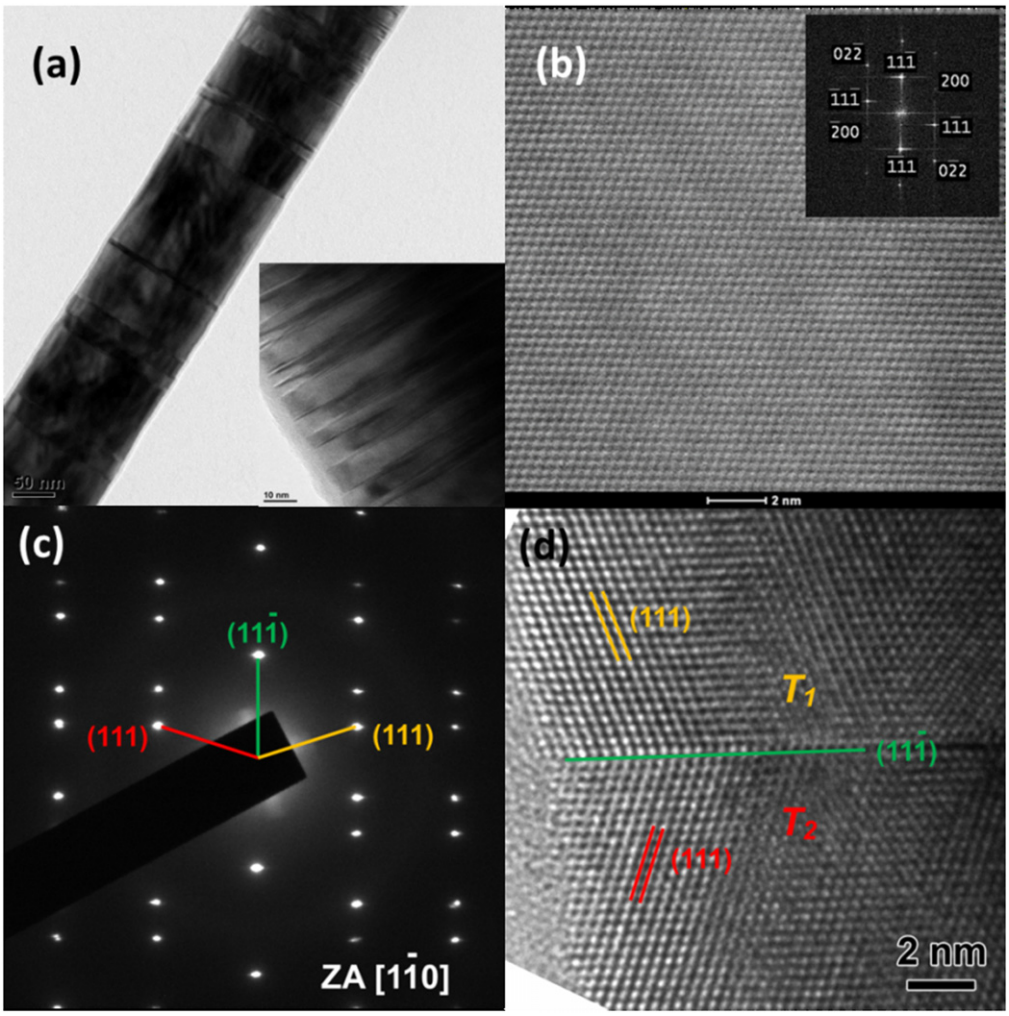

Figure 3. (a) TEM image of core–shell NW, (b) high-resolution STEM image and FFT (inset) acquired using [011] zone axis, (c) SAED pattern shows ZB structure with twins, and (d) HR-TEM image displays the twinning plane (indicated by a green line).

280 nm as the Sb content increases from 3 to 26 at.%, respectively, for similar growth duration. These changes in morphology and diameter are most likely associated with the thermodynamic and kinetic modifications created by the surfactant nature of Sb. Higher Sb flux leads to larger Sb coverage on the surface resulting in the reduction in the free energy of the growth surface, which promotes lateral growth via a vapor solid-growth mechanism. Beyond a certain critical threshold of Sb composition, Sb segregation can occur on the surface [17, 18]. This inhomogeneous Sb coverage on the nanowire surface is likely responsible for the growth of a multitude of side facets at 26 at.% Sb composition and a rough surface morphology.

The alignment of the nanowires also changes from vertical to curved with increasing Sb content. Bending of the NW is strongly influenced by Sb content, increasing with Sb content at a specific growth temperature (figure 2). Hence, it can be inferred that bending of the nanowires is predominantly due to strain accumulation on the NW side facets and thus ruling out any contribution from a thermal stress component as the growth temperature was invariant for the growth. Ghalamestani *et al* [11] also observed similar behavior on their GaAsSb/GaAs core–shell nanowires. Further evidence of the increased strain with increasing Sb incorporation in the nanowires is also found using XRD measurements, as discussed later.

Figure 3(a) displays the bright field TEM micrograph of a typical $GaAs/GaAs_{0.88}Sb_{0.12}$ core–shell nanowire, which exhibits both twins and stacking faults. The lattice resolved HR-STEM image along the [011] zone axis in conjunction with the respective fast Fourier transform (FFT) (figure 3(b)) reveals the zinc-blende (ZB) structure of the NW lattice. The SAED pattern (figure 3(c)) taken along the zone axis [1–10] indicates the twinning structure in the nanowire. The HRTEM image of an isolated twinning plane normal to [11–1] the growth axis is demonstrated in figure 3(d) with the two crystal structures mirrored along the (11-1) plane.

Figure 4 depicts the x-ray diffraction patterns of core–shell GaAs/GaAsSb nanowires with varying Sb content. All diffraction peaks were identified using the Joint Committee on Powder Diffraction Standards (JCPDS) standard database. The nanowires exhibit only GaAs (111), GaAsSb (111), GaSb (111), and Si (111) Bragg peaks, and their respective higher-order reflections. The absence of other orientations further

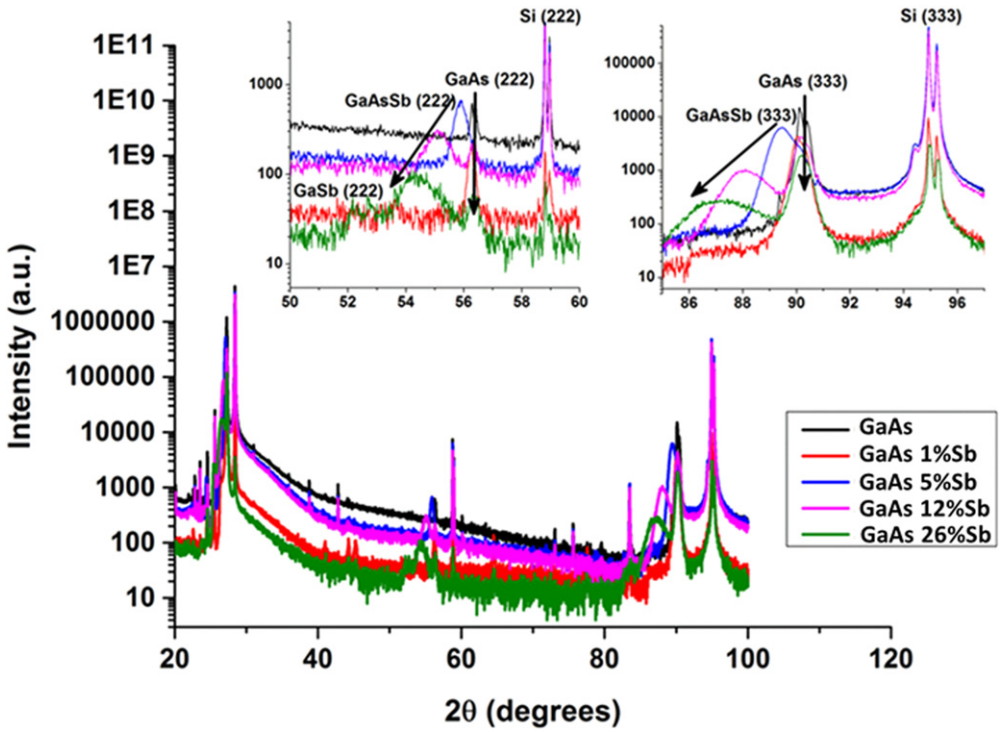

Figure 4. X-ray diffraction patterns of GaAs/GaAsSb nanowires with different Sb compositions.

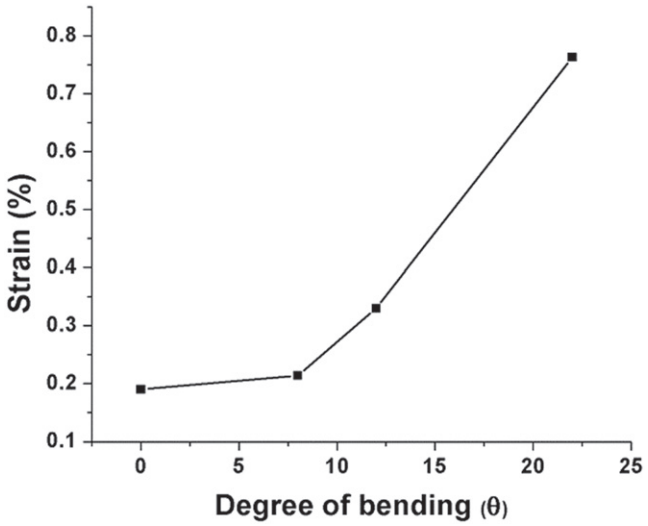

Figure 5. Variation of strain in GaAsSb shell with degree of bending.

attests to the growth of highly vertical <111> oriented nanowires. With increasing Sb composition, the GaAsSb (222) and GaAsSb (333) Bragg peaks shift toward lower angles and are accompanied by significant broadening of the peak as shown in the inset of figure 4. At the highest Sb composition of 26 at.%, pure GaSb phase was observed, which is indicative of the presence of segregated Sb as described above.

Due to close proximity of the first-order (111) peaks of GaAs and GaAsSb in conjunction with the use of an unfiltered Cu K_α source, broadening of the higher-order (222) and (333) GaAsSb reflections was used for estimation of the overall strain in the GaAsSb shell. The strain calculations were estimated by the Williamson–Hall isotropic strain model (W–H ISM) [19, 20] using the total peak broadening. The strain thus calculated was found to increase monotonically with increasing degree of bending as shown in figure 5. These data confirm our earlier conjecture that bending of the nanowires is associated with enhanced strain accumulation in the shell. There are two factors that are likely contributors to this increase in strain. With increasing Sb composition, mismatch between the core and the shell is increased and the shell thickness also increases. Both these lead to increased strain in the shell. Although the Williamson–Hall model has often been used in the literature for determination of the strain in nanowires [19, 21], its applicability for core–shell nanowires is debatable due to non-uniform strain distribution in the shell [22]. As a consequence, while the strain value may not be an absolute value, it provides an overall trend of the strain accumulation in the shell with increasing Sb composition.

Figure 6 shows the normalized micro-photoluminescence (PL) spectra of core–shell nanowires at 4 K for different Sb compositions. The PL spectra of the GaAsSb nanowires reveal emission peaks in the 1.27–0.93 eV spectral range with the specific energies dependent upon the composition. The range shows the red shift with increasing Sb composition from 3 at.% to 26 at.%, and there is an associated peak broadening with increasing Sb content. It is noted that.

GaAs exhibits twin peaks at higher energy of ∼1.47 eV and 1.33 eV, which are identified with the ZB band-to-band transition and As defect (V_{As}) level [23] transition located ∼0.14 eV below the conduction band, respectively.

Since the conduction band (CB) discontinuity is very small in this heterostructure, the change in band gap with increasing Sb content is predominantly accommodated by the

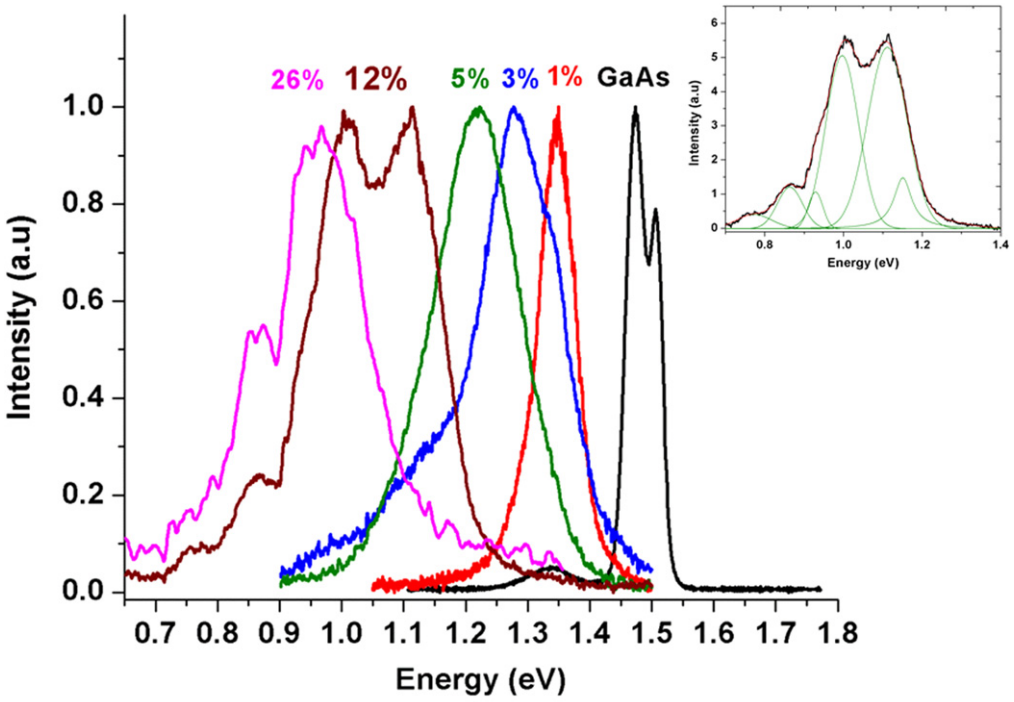

Figure 6. Photoluminescence spectra of GaAs/GaAsSb nanowires with different Sb compositions (inset: deconvolution of peaks for 12 at.% Sb composition).

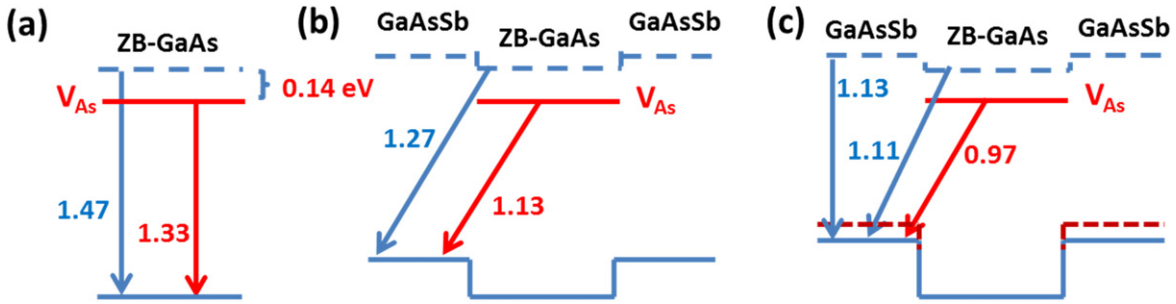

Figure 7. Proposed schematic energy band diagram of (a) ZB GaAs, (b) GaAs/$GaAs_{0.97}Sb_{0.03}$, and (c) GaAs/$GaAs_{0.88}Sb_{0.12}$ (only a few transitions are shown and the dotted line in the VB corresponds to the 2nd Sb composition).

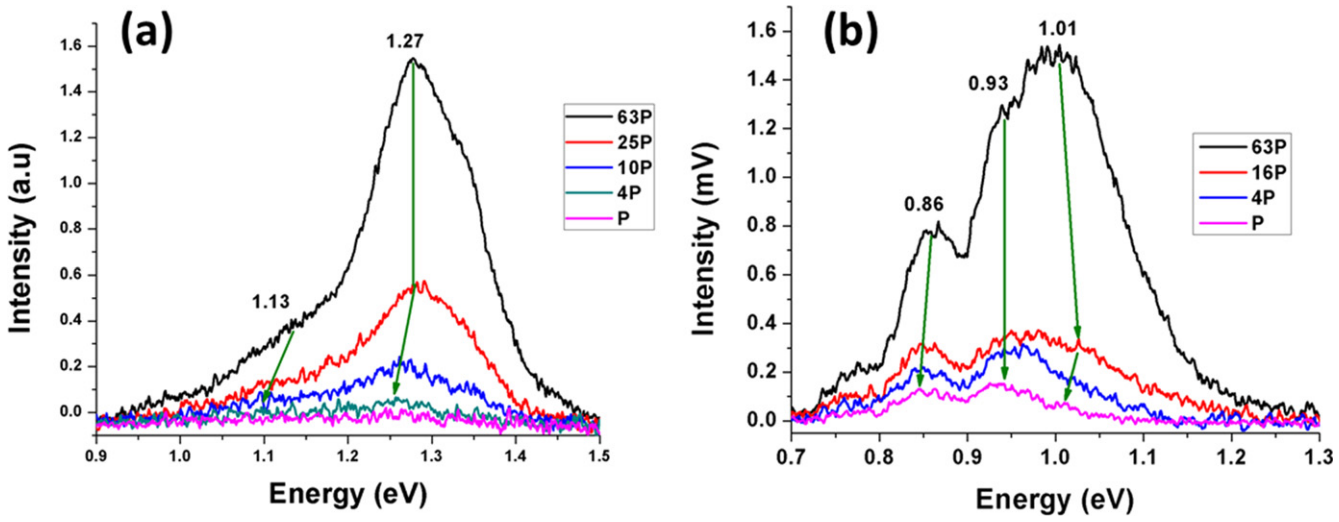

Figure 8. Excitation power dependence PL of (a) GaAs/$GaAs_{0.97}Sb_{0.03}$ and (b) GaAs/$GaAs_{0.74}Sb_{0.26}$ nanowires.

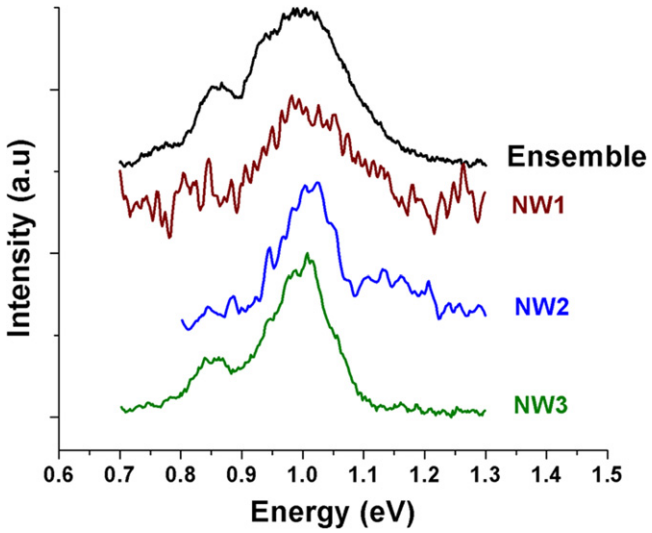

Figure 9. Comparison of the PL spectra for single and ensemble of nanowires.

increasing valence-band (VB) offset [24]. An estimation of the VB offset was made using the simulation software Optel ZB, which provides the evaluation of this offset through interpolation of the VB edges for compound semiconductors [25, 26]. The nature of the transitions was inferred from the excitation power dependence of the 4 K PL spectra discussed below. These were then used to develop the proposed band alignment depicted in figure 7.

Figure 8 displays the excitation power dependence PL for $GaAs/GaAs_{0.97}Sb_{0.03}$ and $GaAs/GaAs_{0.74}Sb_{0.26}$ nanowires. Although data on only two samples at the two extremes of Sb composition range are presented, the intensity dependence was conducted on all the samples discussed earlier over the entire composition range. For 3 at.% Sb, a Gaussian fit to the observed PL spectra results in two peaks at 1.27 eV and 1.13 eV (figure 8(a)) exhibiting a blueshift of ∼20–30 meV with increasing incident PL power by 60x (P is used to denote the lowest baseline intensity, which was 0.5 mW). Such large blue shifts are a signature of type II heterostructures, which is caused by confinement of carriers in a narrow well width due to electric field-induced band bending [27, 28]. The electric field is created by the spatial separation of electron and hole pairs in these structures. Thus, the two transitions we observe are assigned to ZB GaAs CB to GaAsSb VB and V_{As} defect level to GaAsSb VB, respectively. PL spectra of 12 at.% Sb composition are characterized by multitude of peaks occurring at 1.13 eV, 1.11 eV, 1.0 eV, 0.97 eV, and 0.86 eV (inset of figure 6). Except for the 1.13 eV transition, all the transitions are type II in nature due to the blue shift of ∼20 meV observed with the increase in incident power. The presence of two pairs of PL peaks suggests the existence of two different Sb compositions. Peaks at 1.11 eV and 0.97 eV are assigned to a CB of GaAs to VB of GaAsSb and V_{As} to GaAsSb VB, respectively, of one composition and the other two, 1.0 eV and 0.86 eV, for similar transitions corresponding to a second composition in the 12 at.% Sb nanowires. The shoulder on the highest energy peak at 1.13 eV is assigned a transition inside the GaAsSb shell itself. The invariance of the peak with incident excitation power was used to determine the type I nature of this transition. For Sb composition of 26 at.%, PL peaks were observed at 1 eV, 0.93 eV, 0.86 eV, and a weak peak near 0.75 eV as shown in figure 8(b). The dominant peak at 0.93 eV does not exhibit any shift with excitation intensity (figure 8(b)) suggesting a direct band-to-band type I transition in GaAsSb, while the 1 and 0.86 eV emission peaks are identical to those observed in the 12 at.% Sb composition nanowires. Thus, both direct and indirect radiative transitions are present and are excitation-level dependent, with the direct transition dominating at lower excitation level. Finally, the small peak observed at ∼0.75 eV is most likely due to the presence of GaSb phase, which is consistent with the XRD data discussed above.

Figure 9 compares the PL spectra for a selection of nanowires with that for a single NW. Reasonable replication

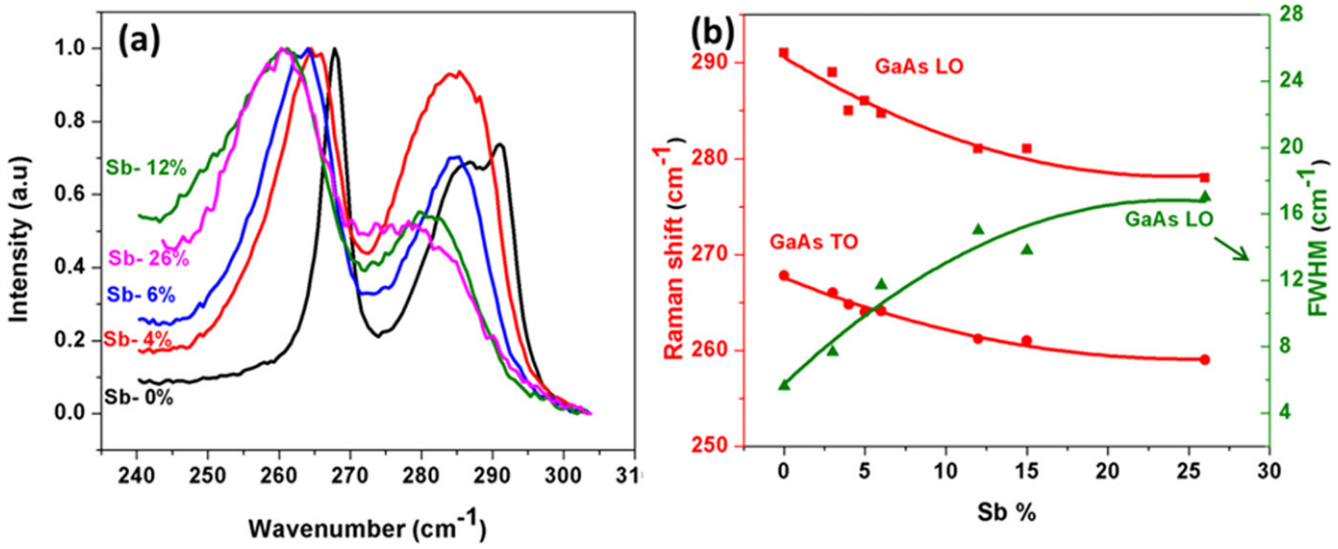

Figure 10. (a) Raman spectra of GaAs/GaAsSb core–shell nanowires and (b) Raman shift and FWHM of core–shell nanowires for different Sb compositions.

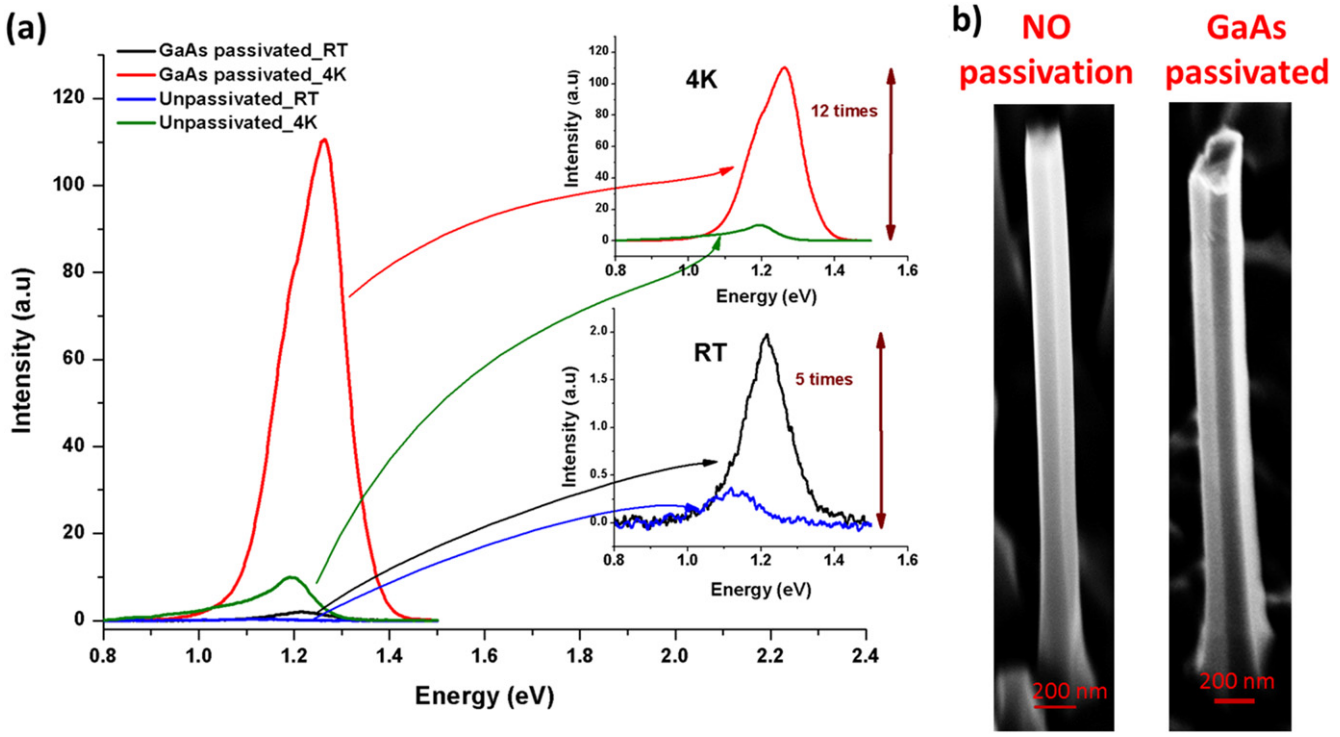

Figure 11. (a) Photoluminescence spectra of GaAs/GaAsSb/GaAs and GaAs/GaAsSb core–shell nanowires and (b) SEM image of GaAs/GaAsSb and GaAs/GaAsSb/GaAs core–shell structured nanowires.

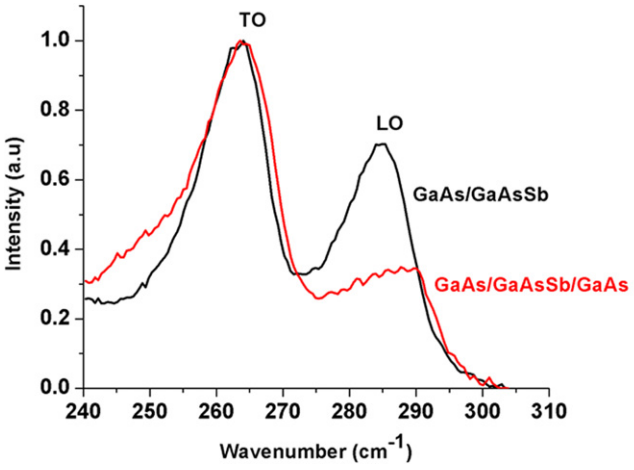

Figure 12. Comparison of the Raman spectra of GaAs/GaAsSb and GaAs/GaAsSb/GaAs nanowires.

of the low-temperature PL of the NW ensemble is observed in the single NW, which attests to the homogeneous composition of these nanowire ensembles. It is commonly reported [29] that the line width of the PL peak in core–shell nanowires is larger due to the electron leakage to the shell. In particular, in the GaAs/GaAsSb system, it is expected to be more pronounced due to the weak electron confinement in the GaAs core. In addition, inhomogeneous strain in the shell, which is enhanced for larger mismatch and higher shell thickness (as is the case in our samples) with increasing Sb composition, also contributes to the increased linewidth. Stacking faults and surface defects are also contributors to the PL broadening [30].

Figure 10(a) shows the room-temperature Raman spectra of core–shell GaAs/GaAsSb nanowires with increasing Sb composition. The Raman spectra of reference GaAs nanowires display longitudinal optical (LO) and transverse optical (TO) modes at 291 cm^{-1} and 267.8 cm^{-1}, respectively, which corresponds to the ZB structure. A shoulder on the LO mode is observed only in the reference sample at 287 cm^{-1} and is attributed to a surface optical mode (SO) [31, 32], which has been commonly observed in thin nanowires. This is not observed in any of the GaAsSb nanowires most likely due to the larger diameter of the core–shell nanowires. A red shift in both the TO and LO modes is observed, which is accompanied by an increase in the full width at half maximum (FWHM) with increasing Sb content, as shown in figure 10(b). The onset of significant asymmetric broadening in Raman peaks and suppression of the LO mode at 12 at.% suggests degrading quality of the nanowires due to the increased strain and compositional inhomogeneity, which is consistent with the XRD and PL observations.

Lastly, a significant improvement in PL intensity has been demonstrated in a double-shell NW configuration, in which an additional GaAs shell is grown around the GaAs/$GaAs_{0.94}Sb_{0.06}$ core–shell nanowires. Similar results were also reported for GaP/GaNP/GaNP core/shell/shell nanowires [33]. The diameter of the double shell is also found to be larger, ∼200 nm, as expected (figure 11(b)). The PL intensity of the dominant peak (∼1.2 eV) is enhanced 12-fold at 4 K and 5-fold at room temperature with respect to the corresponding GaAs/GaAsSb core/shell configuration

(figure 11(a)). Room temperature emission is not often observed at this Sb content for the single-shell configuration but is consistently observed in the double-shell NW configuration. The increased intensity is attributed to the annihilation of the surface defects on the GaAsSb shell. Figure 12 shows a comparison of the Raman spectra of single- and double-shell configured nanowires. The GaAs LO mode is significantly suppressed in the double-shell configuration and is attributed [34] to the LO mode being forbidden from certain surface facets as opposed to no such restrictions imposed on the TO phonon modes. The presence of the LO mode in the single-shell configuration is most likely associated with defects modulating the selection rules to enable the LO mode, normally forbidden, to be observed. Thus, the absence of the LO mode in the double-shell configuration may be viewed as evidence of reduced defects.

It should be noted that these are the preliminary results and GaAs as an outer shell is not an ideal passivating material due to the small conduction band offset between GaAsSb and GaAs and its comparatively low band gap. However, significant enhancement observed in intensity with the use of GaAs outer shell is very promising and indicates future prospects for much improvement in PL efficiency with the use of an appropriate higher band-gap material, namely GaAlAs, as an outer shell material. Also, further tailoring of the growth parameters as well as shell thickness can have a significant effect on improving the PL efficiency.

4. Conclusions

A detailed investigation was carried out on GaAs/GaAsSb core–shell nanowires grown by Ga-assisted MBE intended for next-generation photodetectors in the near-IR spectral regime. These are the first preliminary reports to the best of our knowledge on achieving low PL peak energy of 0.93 eV on these nanowires. The nanowires exhibit a ZB structure, and planar defects, namely twins and stacking faults, are observed. For 12 at.% Sb content and beyond, evidence of compositional instability is observed, resulting in the increased strain accumulation in the shell leading to rough surface morphology, multi-faceted growths, curved nanowires, and deterioration in the structural and optical quality. The type of the optical transitions observed are dependent on the Sb content; a type II transition is seen at low Sb content while a mixture of type I and type II transitions occur at 12 at.% Sb content and beyond. Fairly good replication of the low-temperature photoluminescence spectra of the nanowire ensemble compared to that of a single nanowire attest to the compositional uniformity of the nanowires. Significant enhancement in the PL intensity observed with the passivation of surface defects by implementing a double-shell configuration provides a pathway for future improvement.

Acknowledgments

This work is supported by the Army Research Office (Grant No. W911NF-11-1-0223, technical monitor-William Clark). The authors would like to acknowledge Dr Cynthia S Day, Wake Forest University Chemistry Department x-ray Facility for data collection, and Dr Artur Braun, Empa Swiss Federal Laboratories for Materials Science and Technology for helpful discussions on Williamson–Hall analysis. The authors acknowledge the use of the Analytical Instrumentation Facility (AIF) at North Carolina State University, which is supported by the State of North Carolina and the National Science Foundation.

References

[1] Teissier R, Sicault D, Harmand J C, Ungaro G, Le Roux G and Largeau L 2001 *J. Appl. Phys.* **89** 5473
[2] Hossain N, Hild K, Jin S R, Sweeney S J, Yu S Q, Johnson S R, Ding D and Zhang Y H 2010 *Photonics Global Conf. IEEE* **1**
[3] Hwang J S, Tsai J T, Su I C, Lin H C, Lu Y T, Chiu P C and Chyi J I 2012 *Appl. Phys. Lett.* **100** 222104
[4] Jabeen F, Grillo V, Martelli F and Rubini S 2011 *Sel. Top. Quant. Electron.* **17** 794
[5] Chuang L C, Chen R, Sedgwick F G, Ko W S, Ng K W, Tran T D and Chang-Hasnain C 2010 *Conf. on Lasers and Electro-Optics* (San Jose, CA: Optical Society of America) paper CMFF6
[6] Qiu Y, Walther T, Liu H Y, Jin C Y, Hopkinson M and Cullis A G 2008 *Microscopy of Semiconducting Materials* (Netherlands: Springer) p 263
[7] Plissard S, Dick K A, Wallart X and Caroff P 2010 *Appl. Phys. Lett.* **96** 121901
[8] Dheeraj D L, Zhou H L, Moses A F, Hoang T B, van Helvoort A T J, Fimland B O and Weman H 2010 *Nanowires* (InTech)
[9] Kauko H, Grieb T, Bjørge R, Schowalter M, Munshi A M, Weman H, Rosenauer A and van Helvoort A T J 2013 *Micron.* **44** 254
[10] Kauko H, Fimland B O, Grieb T, Munshi A M, Müller K, Rosenauer A and van Helvoort A T J 2014 *J. Appl. Phys.* **116** 144303
[11] Ghalamestani S G, Munshi A M, Dheeraj D L, Fimland B O, Weman H and Dick K A 2013 *Nanotechnology* **24** 405601
[12] Todorovic J, Kauko H, Ahtapodov L, Moses A F, Olk P, Dheeraj D L, Fimland B O, Weman H and van Helvoort A T J 2013 *Semicond. Sci. Technol.* **28** 115004
[13] Iyer S, Reynolds L, Rawdanowicz T, Ojha S K, Kasanaboina P K and Bowen A 2014 *Nanoscience and Nanoengineering: Advances and Applications* ch 3 (Boca Raton, FL: CRC Press) p 31
[14] Kasanaboina P K, Ojha S K, Sami S U, Reynolds L, Liu Y and Iyer S 2015 *Proc. SPIE* **9373** 937307
[15] Kuang Y J, Sukrittanon S, Li H and Tu C W 2015 *Appl. Phys. Lett.* **107** 012101
[16] Araki Y, Yamaguchi M and Ishikawa F 2013 *Nanotechnology* **24** 065601
[17] Anyebe E A, Rajpalke M K, Veal T D, Jin C J, Wang Z M and Zhuang Q 2015 *Nano Res.* **8** 1309
[18] El Kazzi S, Desplanque L, Wallart X, Wang Y and Ruterana P 2012 *J. Appl. Phys.* **111** 123506
[19] Jenichen B, Brandt O, Pfuller C, Dogan P, Knelangen M and Trampert A 2011 *Nanotechnology* **22** 295714

[20] Pavankumar K, Venkateswarlu K, Rameshbabu N and Muthupandi V 2012 *Key Eng. Mater.* **1463** 739
[21] Stanchu H, Kladko V, Kuchuk A V, Safriuk N, Belyaev A, Wierzbicka A, Sobanska M, Klosek K and Zytkiewicz Z R 2015 *Nanoscale Res. Lett.* **10** 51
[22] Palosz B, Grzanka E, Gierlotka S and Stelmakh S 2010 *Z. Kristallogr. Cryst. Mater.* **225** 588
[23] Prucnal S, Gao K, Anwand W, Helm M, Skorupa W and Zhou S 2012 *Opt. Express* **20** 26075
[24] Alberi K, Wu J, Walukiewicz W, Yu K M, Dubon O D, Watkins S P, Wang C X, Liu X, Cho Y J and Furdyna J 2007 *Phys. Rev.* B **75** 045203
[25] Vurgaftman I, Meyer J R and Ram-Mohan L R 2001 *J. Appl. Phys.* **89** 5815
[26] http://users.wpi.edu/∼lrram/Publications/AllPub.html
[27] Chiu Y S, Ya M H, Su W S and Chen Y F 2002 *J. Appl. Phys.* **92** 5810
[28] Morozov S V, Kryzhkov D I, Yablonsky A N, Antonov A V, Kuritsin D I, Gaponova D M, Sadofyev Y G, Samal N, Gavrilenko V I and Krasilnik Z F 2013 *J. Appl. Phys.* **113** 163107
[29] Hussain A M P, Sarangi S N and Sahu S N 2010 arXiv:1004 2319
[30] Zhang G, Tateno K, Birowosuto M D, Notomi M, Sogawa T and Gotoh H 2015 *Nanotechnology* **26** 115704
[31] Esther A L, Conesa-Boj S, Wallart X, Caroff P and Morral A F 2013 *Nanotechnology* **24** 405707
[32] Dobrovolsky A, Sukrittanon S, Kuang Y J, Tu C W, Chen W M and Buyanova I A 2014 *Appl. Phys. Lett.* **105** 193102
[33] Stehr J E, Dobrovolsky A, Sukrittanon S, Kuang Y, Tu C W, Chen W M and Buyanova I A 2015 *Nano Lett.* **15** 242
[34] Begum N, Piccin M, Jabeen F, Bais G, Rubini S, Martelli F and Bhatti A S 2008 *J. Appl. Phys.* **104** 104311